Electronic Supplementary Information

Amide and N-oxide functionalization of T-shaped ligand for isoreticular MOFs with giant enhancement in CO_2 capture and separation

Ying Xiong, Yan-Zhong Fan, Rui Yang, Sha Chen, Mei Pan, Ji-Jun Jiang*, and Cheng-Yong Su*

MOE Laboratory of Bioinorganic and Synthetic Chemistry, Lehn Institute of Functional Materials (LIFM), School of Chemistry and Chemical Engineering, Sun Yat-Sen University, Guangzhou 510275, China, and State Key Laboratory of Applied Organic Chemistry, Lanzhou University, Lanzhou 730000, China.

Table of contents

1. General Procedures, Materials, and Instrumentation

2. Synthesis of Ligands and Complexes

3. Single-crystal Analyses

4. TG, IR and PXRD Characterization

5. Sorption Property and Selectivity Calculation

6. Sorption Simulation

7. References

1. Materials and physical measurements

All chemicals were obtained from commercial sources and directly utilized without further purification. Solid-state IR spectra were recorded using Nicolet/Nexus-670 FT-IR spectrometer in the region of 4000−400 cm^{-1} using KBr pellets. Mass spectra (MS) were recorded on a JEOL accuTOF CS JMS-T100CS mass spectrometer. Elemental analyses were performed by Perkin-Elmer 240 elemental analyzer. Powder X-ray diffraction (XRD) measurements were performed on a Bruker D8 ADVANCE diffractometer at 40 kV and 40 mA with a Cu target tube and a graphite monochromator. Gas adsorption isotherms for pressures in the range of 0-1.0 bar were obtained by a volumetric method using a quantachrome autosorb-iQ2-MP gas adsorption analyzer. Gas adsorption measurements were performed using ultra-high purity N_2, CO, CO_2 and CH_4 gases. ^{1}H NMR spectra were measured with a Varian Mercury Plus 300 MHz spectrometer.Thermogravimetric analysis (TGA) was performed on a NETZSCH TG209 system in nitrogen and under 1 atm of pressure at a heating rate of 10 °C min^{-1}.

2. Synthesis of ligands and complexes

5-(Isonicotinoylamino)isophthalic acid(H_2INIA)

The **H_2INIA**ligand was prepared according to the literature.[1] Yield: 60%. ^{1}H-NMR (300 MHz, D_6-DMSO, 25°C): δ =10.80(s, 1H), 8.79-8.77(d, 2H, J=6.0 Hz), 8.64 (s, 2H), 8.22(s, 1H), 7.89-7.87(d, 2H, J=6.0).

5-(Isonicotinoylamino N-oxide)isophthalic acid(H_2INOIA)

The **H_2INOIA** ligand was prepared according to the literature[1]by changing the isonicotinic acid withisonicotinic acid N-oxide.Yield: 75.5%. ^{1}H NMR (300 MHz, D_6-DMSO, 25℃): δ =10.69(s, 1H), 8.62 (s, 2H), 8.38-8.36 (d, 2H, J=6.0 Hz), 8.20(s, 1H), 8.00-7.98(d, 2H, J=6.0 Hz).

Synthesis of [Cu(INIA)]·2.5DMF·2H_2O (LIFM-10(Cu))

A mixture of 0.2 mmol of $Cu(NO_3)_2$ and 0.1 mmol of **H_2INIA** was dissolved in 8 mL of DMF,and heated at 60 ℃ for 5 min to result in blue floccules. Then the system was added 2 drops of $HNO_3$to give green clear solvent. The solvent was transferred to a 15 mL Teflon-lined stainless steel vessel and heated at 80 °C for 60h, then cooled to 30 ℃ at a rate of 10 ℃/100 min. The green powder formed were collected by filtration and washed by DMF for

several times. Yield:80.4 %. IR (KBr, cm^{-1}): 3436(s), 1673(m), 1617(s),1585(m), 1564(s), 1416(m), 1383(s), 1286(s), 779(w), 722(w). Elemental analysis (% calc/found): C: 45.58/45.33, H: 5.25/5.37, N: 11.13/11.18.

Synthesis [Cu(INOIA)]·2DMF·3H_2O (LIFM-11(Cu))

A mixture of 0.2 mmol of $Cu(NO_3)_2$ and 0.1 mmol of **H_2INOIA** was dissolved in 8 mL of DMF, and heated in a 15 mL Teflon-lined stainless steel vessel at 80 °C for 60h, then cooled to 30 ℃ at a rate of 10 ℃/100 min. The green powder formed were collected by filtration and washed by DMF for several times.Yield:78.3%. IR (KBr, cm^{-1}): 3436(m), 1713(m)，1672(m), 1636(m),1585(m), 1563(m), 1489(w), 1434(m), 1374(s), 1292(w), 1228(m), 1095(w), 865(w), 774(w), 729(w), 589(w), 487(w). Elemental analysis (% calc/found): C: 42.04/42.59, H: 5.16/5.00, N: 11.38/9.93.Single crystals of **LIFM-11(Cu)** were grown as following: 0.2 mmol of $Cu(NO_3)_2$ and 0.1 mmol of **H_2INOIA** was added to DMF (5 mL) to lead to green precipitation. Dissolving the precipitant with one drop of HNO_3 (16 mmol/L), then transfered the green liquid to test tube and kept it still. Green single crystals produced after two weeks. Yield: 25.3%.

3. Crystal structure determination

Single crystals of**LIFM-10(Cu)** and **LIFM-11(Cu)** were carefully picked and coated in paratone oil, attached to a glass silk inserted in a stainless steel stick, then quickly transferred to the Agilent Gemini S Ultra CCD Diffractometerwith the Enhance X-ray Source of Cu radiation (λ = 1.54178 Å) using the ω-ϕ scan technique. Structural solution and refinement against F^2 were carried out using the SHELXL programs.[2] Hydrogen atoms were placed in geometrically calculated positions and included in therefinement process using riding model with isotropic thermal parameters: U_{iso}(H) = 1.2U_{eq}(-CH). For all structures the contribution of heavily disordered solvent molecules was treated by the Squeeze procedure implemented in Platon.[3]The pyridine ring and amido group within framework displayed orientationdisorder, therefore, they were located and refined with restraints (DFIX, FLAT, ISOR and SIMU) to have satisfactory displacement parameters. Crystal and refinementparameters are listed in table S1. CCDC 1012810-1012811.

Table S1. Crystallographic data for LIFM-10(Cu) and LIFM-11(Cu)

Compound	**LIFM-10(Cu)**	**LIFM-11(Cu)**
Formula	$C_{14}H_8N_2O_5Cu$	$C_{14}H_8N_2O_6Cu$
Formula weight	347.76	363.76
T (K)	150.15	150.15
Crystal system	Trigonal	Trigonal
Space group	$R\bar{3}$	$R\bar{3}$
a (Å)	18.9171(15)	18.569(3)
b (Å)	18.9171(15)	18.569(3)
c (Å)	37.995(5)	40.907(8)
α (°)	90.00	90.00
β (°)	90.00	90.00
γ (°)	120.00	120.00
V (Å^3)	11775(2)	12215(3)
Z	18	18
D_{calc}(g/cm^3)	0.883	0.890
μ/mm^{-1}	1.315	1.312
R_{int}	0.0477	0.0741
R_1	0.0895	0.0761
wR_2	0.2516	0.2375
S	1.039	0.999

Table S2. Selected bond lengths (Å) and angles (°) for LIFM-10(Cu) and LIFM-11(Cu)

LIFM-10(Cu)			
Cu1-N1A	2.194(9)	Cu1-O2#2	1.954(4)
Cu1-N1B	2.182(16)	Cu1-O3#1	1.943(4)
Cu1-O4#4	1.976(4)	Cu1-O5#3	1.967(4)
N(1B)-Cu(1)-N(1A)	9.5(7)	O(2)#2-Cu(1)-N(1A)	92.2(3)
O(4)#4-Cu(1)-N(1A)	86.6(3)	O(3)#1-Cu(1)-N(1A)	100.7(3)
O(5)#3-Cu(1)-N(1A)	105.8(3)	O(4)#4-Cu(1)-N(1B)	91.9(5)
O(2)#2-Cu(1)-N(1B)	84.4(6)	O(2)#2-Cu(1)-N(1B)	84.4(6)
O(5)#3-Cu(1)-O(4)#4	167.57(17)	O(2)#2-Cu(1)-O(4)#4	89.5(2)
O(3)#1-Cu(1)-N(1B)	108.7(6)	O(3)#1-Cu(1)-O(2)#2	166.85(17)
O(3)#1-Cu(1)-O(5)#3	89.39(19)	O(3)#1-Cu(1)-O(4)#4	89.1(2)
O(2)#2-Cu(1)-O(5)#3	89.21(19)		
Symmetry code for **LIFM-10(Cu)**, #1, -y+4/3,x-y+2/3,z-1/3; #2, y-1/3,-x+y+1/3,-z+1/3; #3, -x+y+1/3,-x+2/3,z-1/3; #4 x-y+2/3,x+1/3,-z+1/3.			
LIFM-11(Cu)			
Cu(1)-O(5)#1	1.971(3)	Cu(1)-O(3)#3	1.975(3)
Cu(1)-O(4)#2	1.973(3)	Cu(1)-O(6)#4	1.978(3)
Cu(1)-O(1)	2.119(3)		
O(5)#1-Cu(1)-O(4)#2	90.39(16)	O(5)#1-Cu(1)-O(6)#4	168.63(13)
O(5)#1-Cu(1)-O(3)#3	88.64(17)	O(4)#2-Cu(1)-O(6)#4	88.67(15)
O(4)#2-Cu(1)-O(3)#3	168.63(13)	O(3)#3-Cu(1)-O(6)#4	90.05(16)
O(4)#2-Cu(1)-O(1)	95.33(14)	O(5)#1-Cu(1)-O(1)	95.51(15)
O(3)#3-Cu(1)-O(1)	96.04(15)	O(6)#4-Cu(1)-O(1)	95.86(14)
Symmetry code for **LIFM-11(Cu)**, #1, x-y-1/3,x-2/3,-z+1/3; #2, -y+1/3,x-y-1/3,z-1/3; #3, y+2/3,-x+y+1/3,-z+1/3; #4, -x+y+4/3,-x+2/3,z-1/3.			

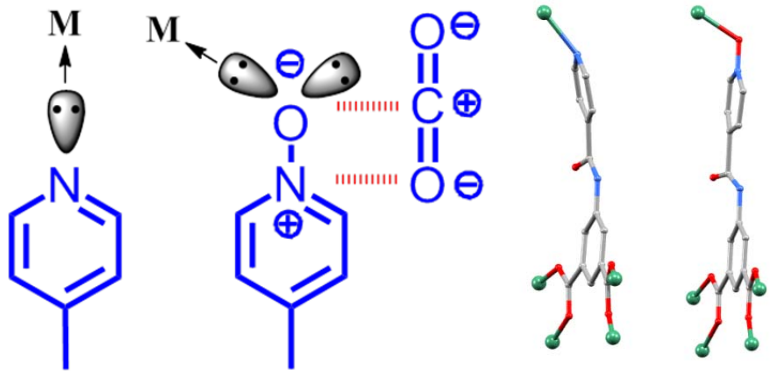

Figure S1. Metal binding modes of pyridyl donor and pyridyl N-oxide donor (left) showing preferential interactions with CO_2, andtheir coordination behaviors in **LIFM-10(Cu)** and **LIFM-11(Cu)** (right).

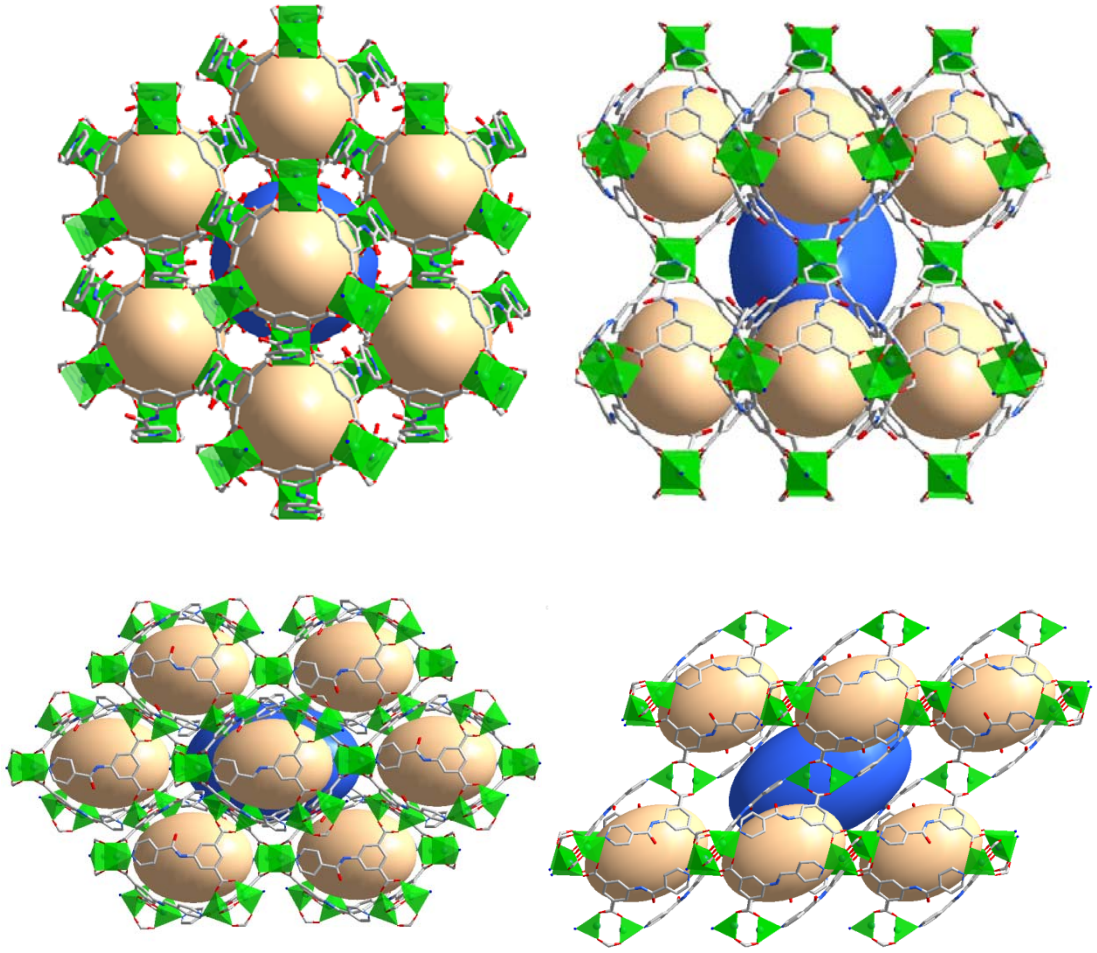

Figure S2. Top and side view of the 3D framework of $ScD_{0.33}$topology in **LIFM-10(Cu)** and **LIFM-11(Cu)** showing hourglass-shapedporous channels.Balls in different colorsshow the 6-nuclear Cu-cage and 12-nuclear Cu-cage inside the channels.

4. TG, IR and PXRD Characterization

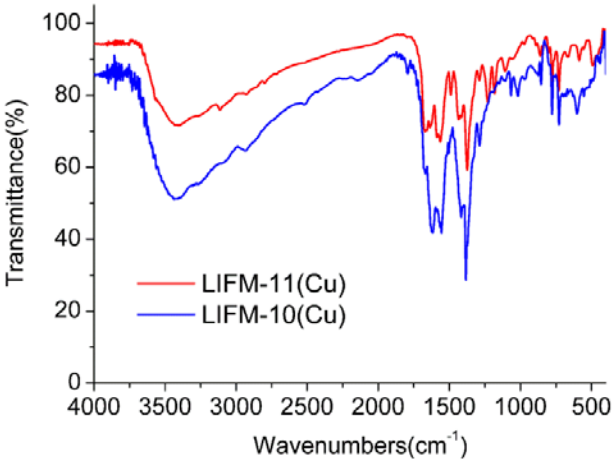

Figure S3.FT-IR spectrums of **LIFM-10(Cu)** and **LIFM-11(Cu)**.

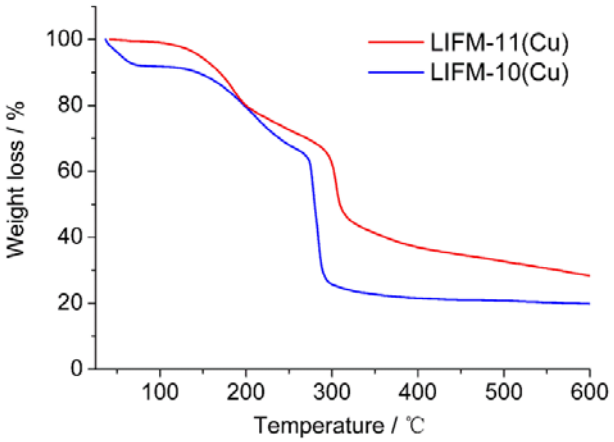

Figure S4. TGA curves of **LIFM-10(Cu)** and **LIFM-11(Cu)**. For **LIFM-10**: 38.66 % (Cal. 38.50 %) weight loss is expected for 2.5 DMF and 2 H_2O molecules;for**LIFM-11**: 35.54 % (Cal. 35.72 %) weight loss is expected for**LIFM-11(Cu)** DMF and 3 H_2O molecules.

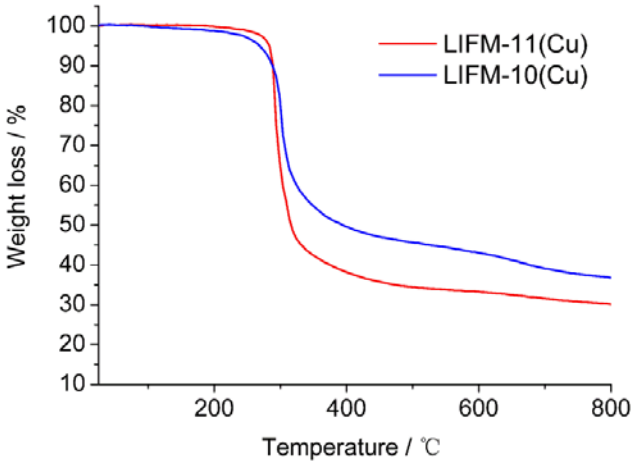

Figure S5. TGA curves of activated**LIFM-10(Cu)** and **LIFM-11(Cu).**

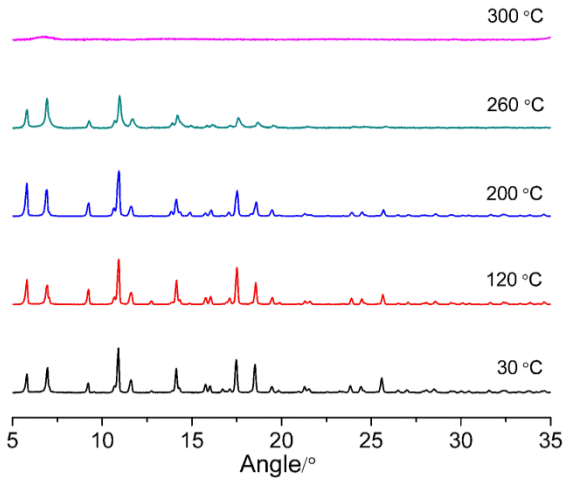

Figure S6. Variable-Temperature dependentpowder X-ray diffraction (PXRD) patterns of **LIFM-10(Cu)**.

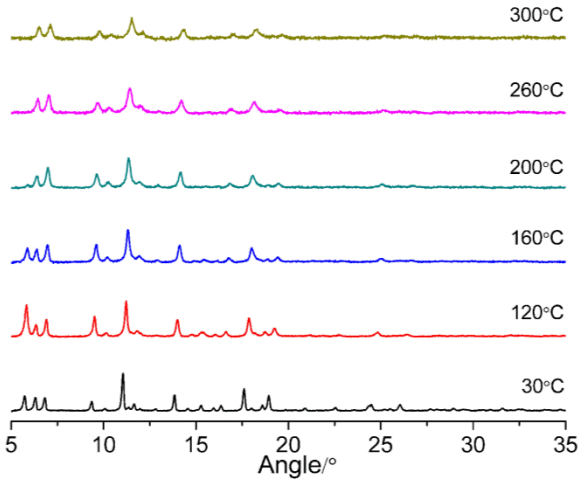

Figure S7. Variable-Temperaturedependent PXRD patterns of **LIFM-11(Cu)**.

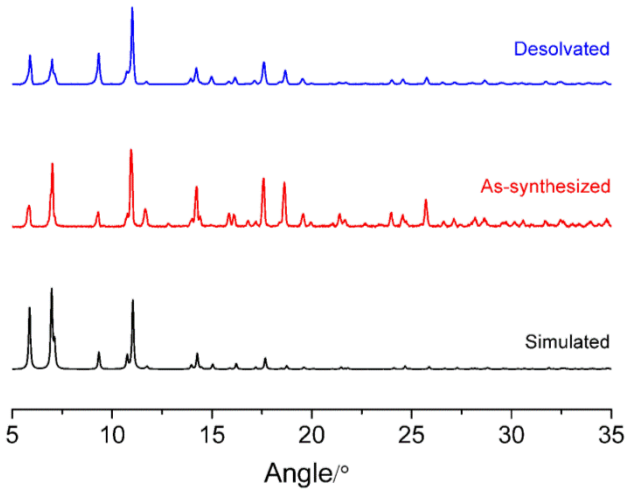

Figure S8. PXRD patterns of **LIFM-10(Cu)**: simulated from single-crystal data, as-synthesized sample and activated sample.

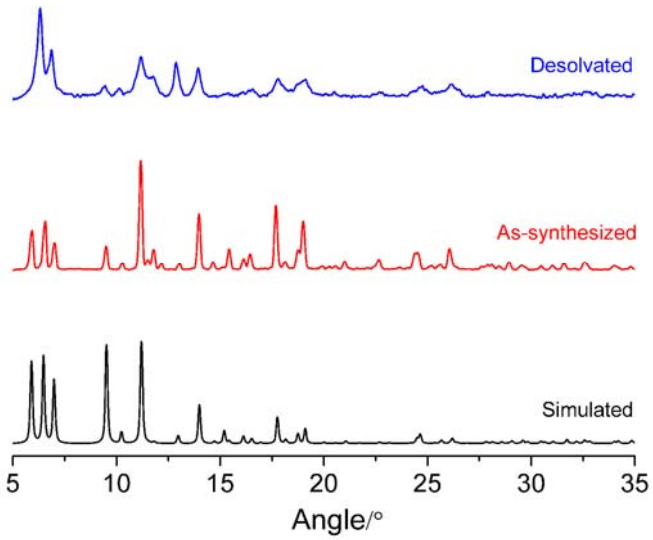

Figure S9. PXRD patterns of **LIFM-11(Cu)**: simulated from single-crystal data, as-synthesized sample and activated sample.

5. Sorption Property and Selectivity Calculation

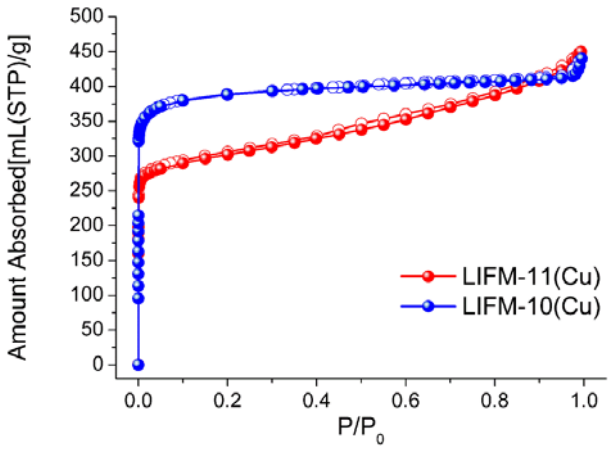

Figure S10. N_2 (77K) sorption isotherms of **LIFM-10(Cu)** and **LIFM-11(Cu)**. Solid symbols: adsorption, open symbols: desorption.

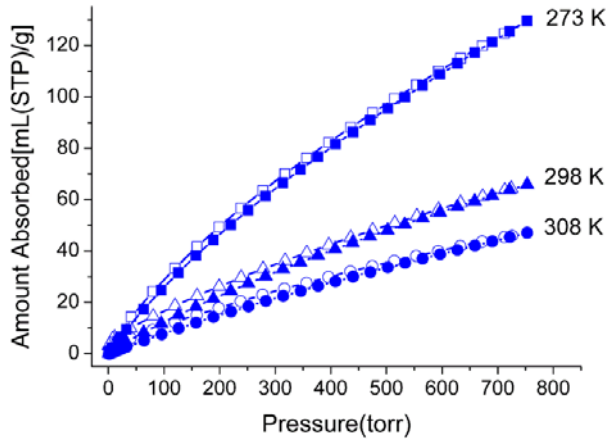

Figure S11.CO_2 (273, 298 and 308 K) sorption isotherms of **LIFM-10(Cu)**. Solid symbols: adsorption, open symbols: desorption.

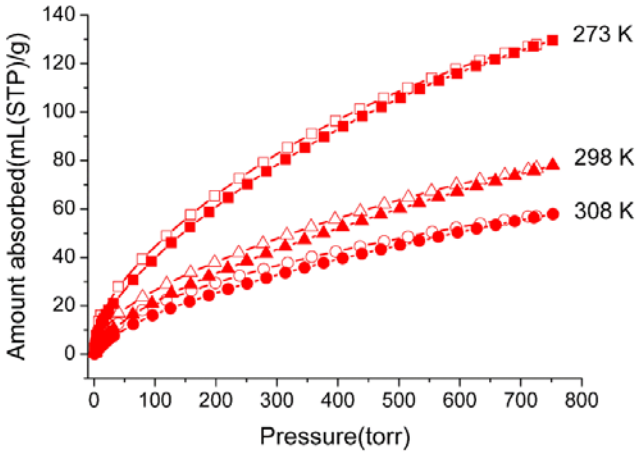

Figure S12.CO_2 (273, 298 and 308 K) sorption isotherms of **LIFM-11(Cu)**. Solid symbols: adsorption, open symbols: desorption.

Calculations of adsorption isosteric heats

The isosteric heats of CO_2 adsorption for **LIFM-10(Cu)** and **LIFM-11(Cu)** were calculated from the sorption data measured at 273, 298, 308 K by the virial fitting method. A virial-type expression (eq. 1) which is composed of parameters a_i and b_i is used. In eq. 1, P is the pressure in torr, N is the adsorbed amount in mmol·g^{-1}, T is the temperature in Kelvin,$a_i$and $b_i$are the virial coefficients which are independent of temperature, and m and n are the numbers of coefficients required to adequately describe the isotherms.

$$\ln P = \ln N + \frac{1}{T}\sum_{i=0}^{m} a_i N^i + \sum_{i=0}^{n} b_i N^i \qquad \text{eq. 1}$$

The values of the virial coefficients a_0 through a_m were then applied to calculate the

isosteric heat of adsorption (eq 2). In eq. 2, Q_{st} is the coverage-dependent isosteric heat of adsorption and R is the universal gas constant.[4]

$$Q_{st} = -R\sum_{i=0}^{m} a_i N^i \qquad \text{eq. 2}$$

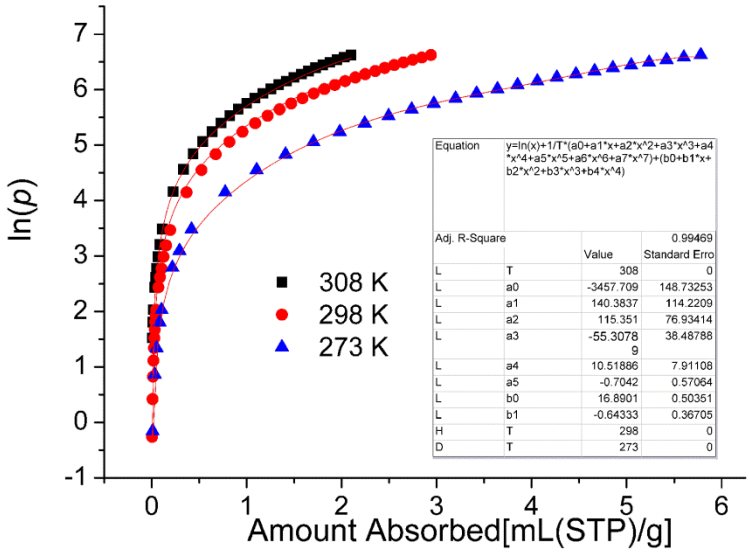

Figure S13. Virial fitting (lines) of the CO_2 adsorption isotherms (points) of **LIFM-10(Cu)** measured at 273 K, 298 K, and 308 K

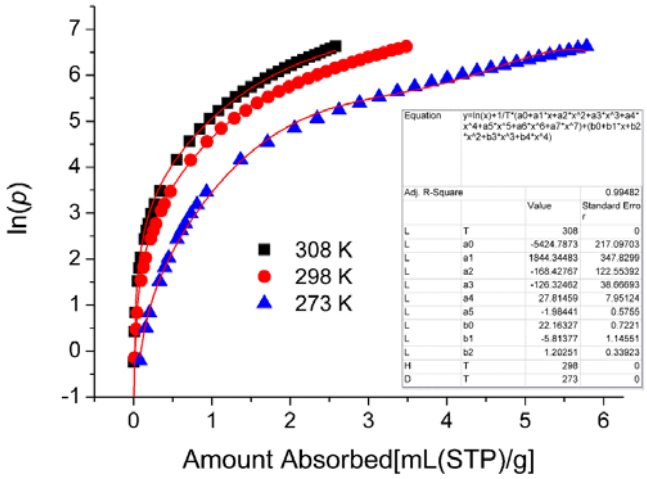

Figure S14. Virial fitting (lines) of the CO_2 adsorption isotherms (points) of **LIFM-11(Cu)** measured at 273 K, 298 K, and 308 K.

Table S3 Zero-Coverage isosteric heat of CO_2adsorption of MOFs

Compound (common name)	*Q*st (kJ /mol)	Functionality type	Reference
Cu-BTTri-mmen	96	amines	5
Cu-BTTri-en	90	amines	6
Zn(DCTP)(DABCO)	77	amines	7
MIL-100(Cr)	62	Open metal sites	8
TBA@bio-MOF-1	55	amines	9
LIFM-11(Cu)	**53**	**Amide and N-oxide**	This work
NH_2-MIL-53(Al)	50	amines	10
CAU-1	48	amines	11
Mg-MOF-74, CPO-27-Mg	47	Open metal sites	12
bio-MOF-11	45	amines	13
MIL-101(Cr)	44	Open metal sites	8
Ni-MOF-74	42	Open metal sites	14
LIFM-10(Cu)	**29**	**Amide**	**This work**

Calculations of adsorption selectivity

Ideal adsorbed solution theory(IAST) developed by Myers and Prausnitz[15] was used to estimate the selectivities of CO_2/N_2 (15:85), CO_2/CO (50:50) and CO_2/CH_4 (50:50) mixture compositions from their respective single-component isotherms. The CO_2, N_2 and CH_4 isotherms were fitted to the single-site Langmuir equation and the CO isotherms to the dual-sites Langmuir equation. Selectivities were then calculated according to eq. 3, where $x_i$is the mole fraction of component i in the adsorbed phase and y_i is the mole fraction of component i in the bulk.

$$S = \frac{x_i y_i}{x_j y_i} \qquad \text{eq. 3}$$

Adsorption selectivities can also be calculated by a virial fitting method based on the following equation:

$$\ln N/P = A_0 + A_1 N + A_2 N^2 + A_3 N^3 + \cdots \qquad \text{eq. 4}$$

In eq. 4, P is pressure, N is amount adsorbed and A_0, A_1 etc. present virial coefficients. A_0 is related to adsorbate–adsorbent interactions, and A_1 describes adsorbate–adsorbate interactions. The Henry's Law constant (K_H) is equal to exp(A_0).

The Henry's Law selectivity for gas component i over j is calculated based on eq. 5:[16]

$$S_{ij} = K_{Hi}/K_{Hj} \qquad \text{eq. 5}$$

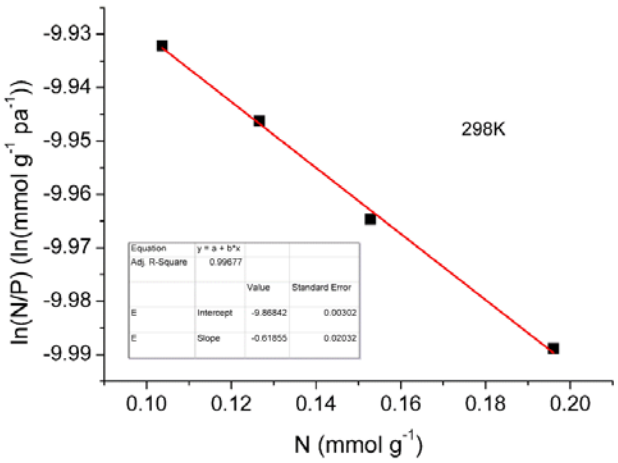

Figure S15. The virial graphs for adsorption of CO_2 on **LIFM-10(Cu)**.

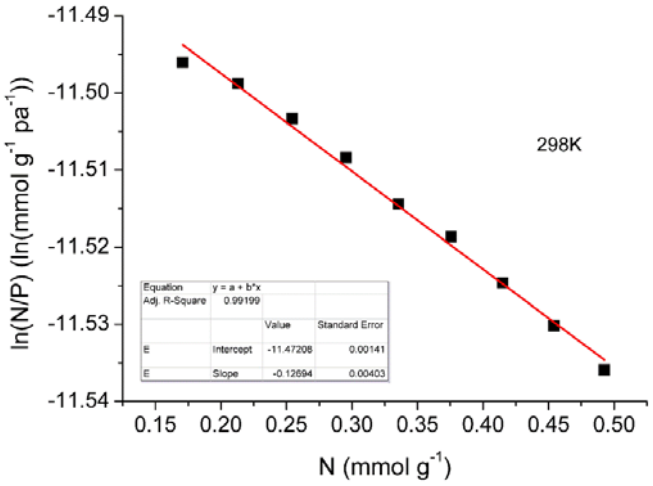

Figure S16. The virial graphs for adsorption of CH_4 on **LIFM-10(Cu)**.

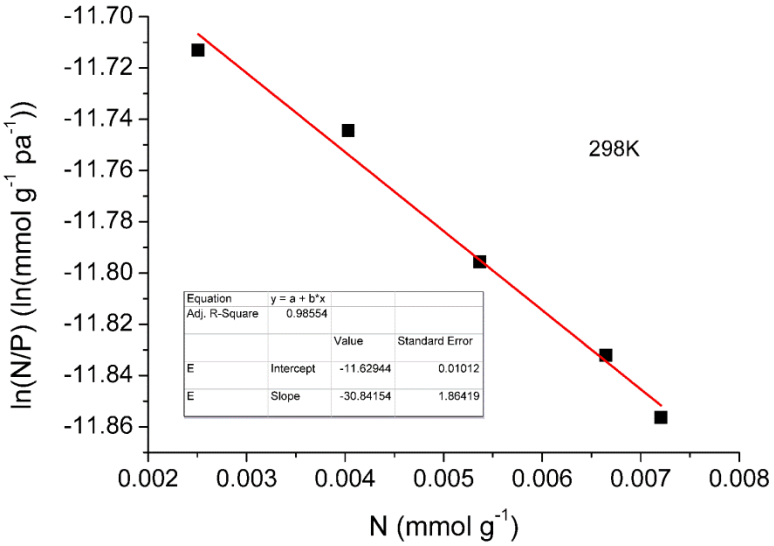

Figure S17. The virial graphs for adsorption of CO on **LIFM-10(Cu)**.

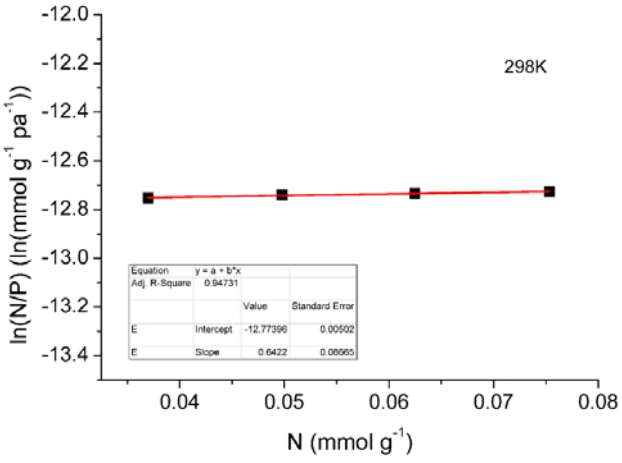

Figure S18. The virial graphs for adsorption of N_2 on **LIFM-10(Cu)**.

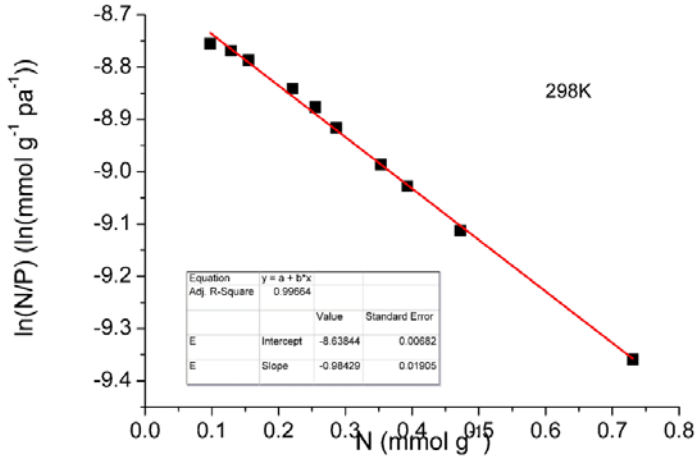

Figure S19. The virial graphs for adsorption of CO_2 on **LIFM-11(Cu)**.

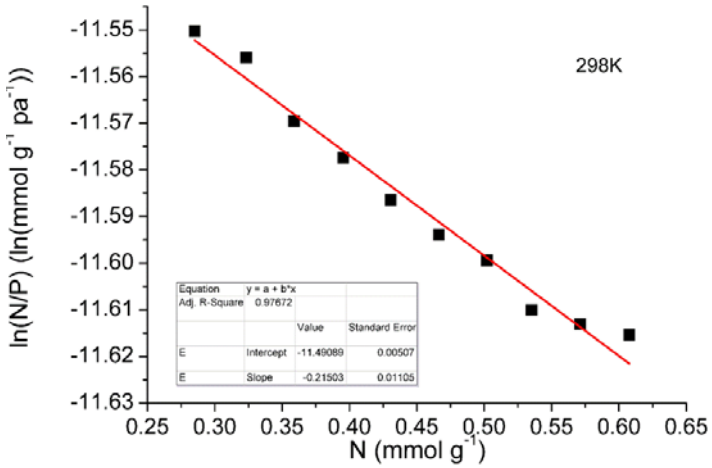

Figure S20. The virial graphs for adsorption of CH_4 on **LIFM-11(Cu)**.

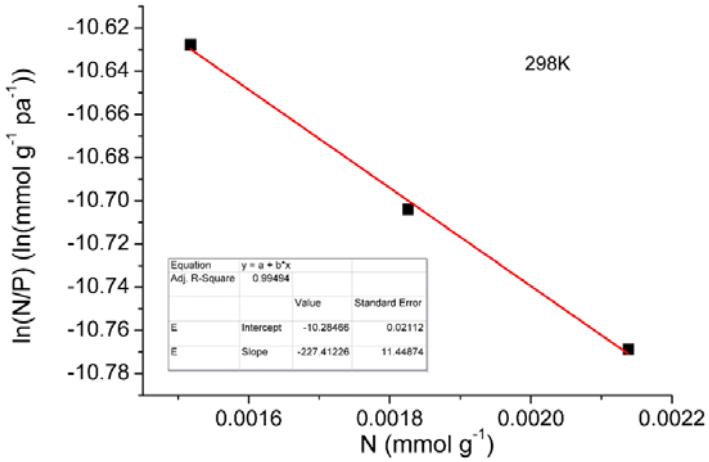

Figure S21. The virial graphs for adsorption of CO on **LIFM-11(Cu)**.

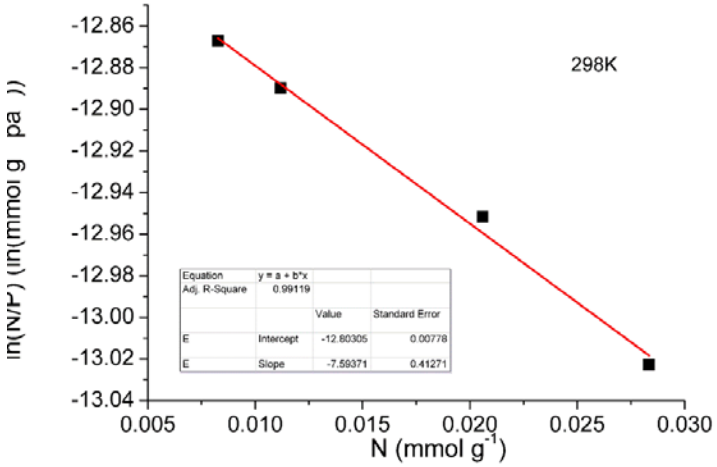

Figure S22. The virial graphs for adsorption of N_2 on **LIFM-11(Cu)**.

Table S4 Virialgraph analyses data for **LIFM-10(Cu)** and its CO_2/CH_4, CO_2/CO and CO_2/N_2separation selectivities at 298 K

Adsorbate	**T/K**	K_H/**mol g^{-1} torr^{-1}×10^{-3}**	**a_0/ln(mol g^{-1} torr^{-1})**	**b_0/ln(mol g^{-1} torr^{-1})**	S_{ij}
CO_2	298	0.0518	-9.868±0.003	-0.619±0.020	——
CH_4	298	0.0104	-11.472±0.001	-0.127±0.004	4.98
CO	298	0.00890	-11.629±0.010	-30.842±1.864	5.82
N_2	298	0.00283	-12.774±0.009	-0.642±0.087	18.30

[a]The Henry's law selectivity for gas component CO_2 over *i*is calculated based on the equation $S_{ij} = K_H(CO_2)/K_H(i)$.

Table S5 Virialgraph analyses data for**LIFM-11(Cu)** and its CO_2/CH_4, CO_2/CO and CO_2/N_2separation selectivities at 298 K

Adsorbate	**T/K**	K_H/**mol g^{-1} torr^{-1}×10^{-3}**	**a_0/ln(mol g^{-1} torr^{-1})**	**b_0/ln(mol g^{-1} torr^{-1})**	S_{ij}
CO_2	298	0.177	-8.638±0.007	-0.984±0.019	——
CH_4	298	0.0102	-11.491±0.005	-0.215±0.011	17.35
CO	298	0.0342	-10.284±0.021	-227.412±11.445	5.18
N_2	298	0.00275	-12.803±0.008	-7.594±0.413	64.36

[a]The Henry's law selectivity for gas component CO_2 over *i*is calculated based on the equation $S_{ij} = K_H(CO_2)/K_H(i)$.

6. Sorption Simulation

DFT-ESP charge

Two MOFs got from single-crystal data were intercepted to discrete paddle-wheel clusters, calculating their ESP (electrostatics potential) charges.[17]The density functional theory (DFT) method was employed using the B3LYP hybrid functional.[18] Clusters were calculated with a basis set consisting of LANL2DZ basis set[19] for Cu, while the 6-31+G* basis set for C, H, O and N. All the calculation was performed with Gaussian 09[20] package. The ESP charges were signed beside the atoms of ligands in Fig S23.

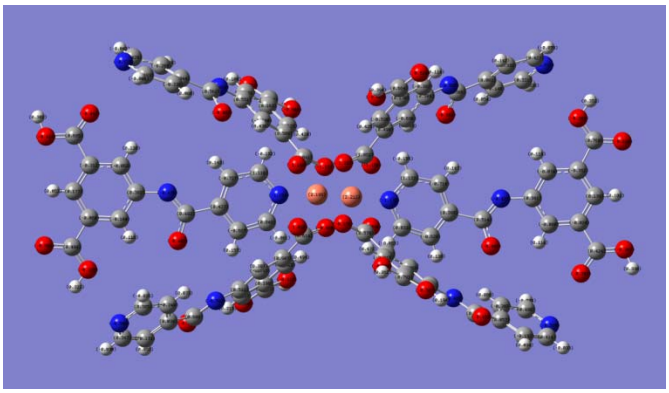

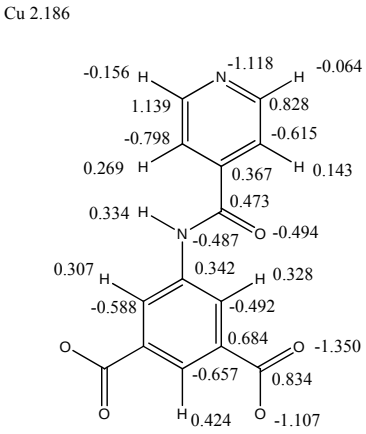

Partial atomic charge of LIFM-10(Cu)

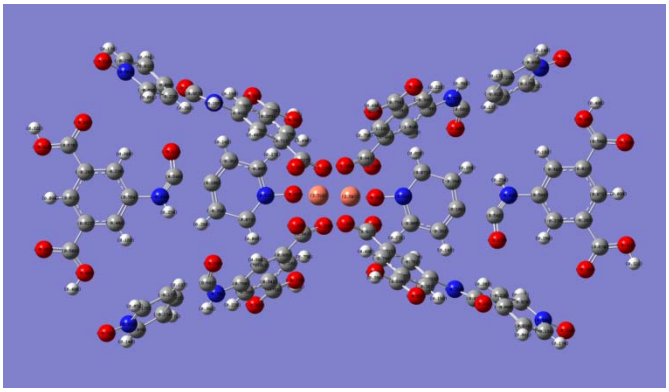

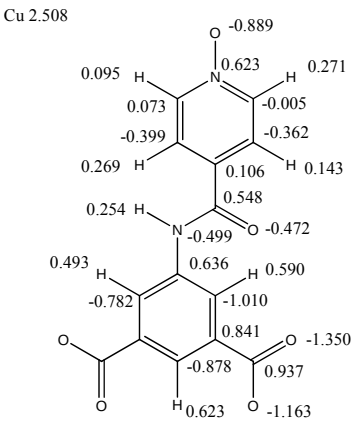

Partial atomic charge of **LIFM-11(Cu)**

Figure S23. ESP charges and structure of ligands (**LIFM-10(Cu)** and **LIFM-11(Cu)**)

Annealing simulation method

Simulated annealing techniques[21] were used to search the adsorption sites by Monte Carlo method. Each simulation is composed of 10 cycles and each cycle consists of 3×10^6 steps. In each cycle, the system was heated up to 627 K and then slowly cooled down to 298 K. The information of thermo-stable geometry structure would be gained as the unstable sites were eliminated by the high temperature.

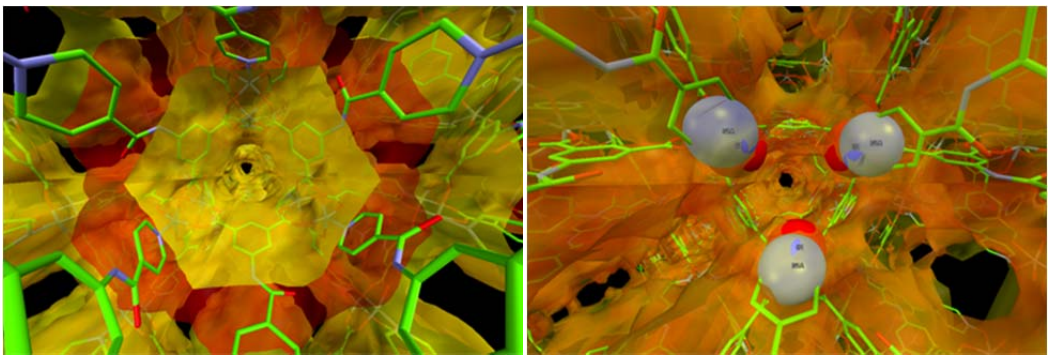

Figure S24. Inside view of voids in **LIFM-10(Cu)**(left)with pyridylamino and carboxylate groups and **LIFM-11(Cu)**(right) with N-oxide groups on the pore surface.

LIFM-10(Cu)	**LIFM-11(Cu)**
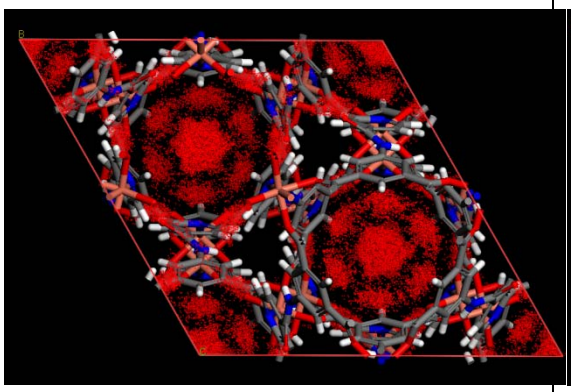	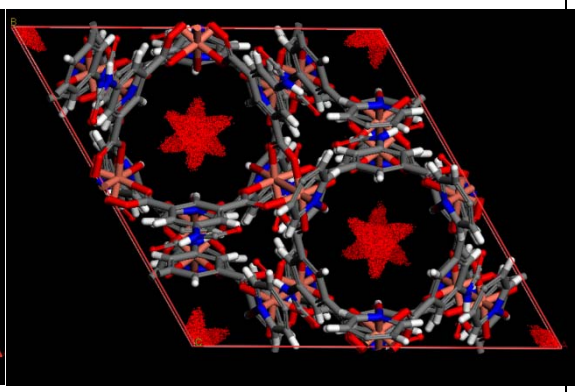
CO_2 distribution, viewed from *c* axis	CO_2 distribution, viewed from *c* axis
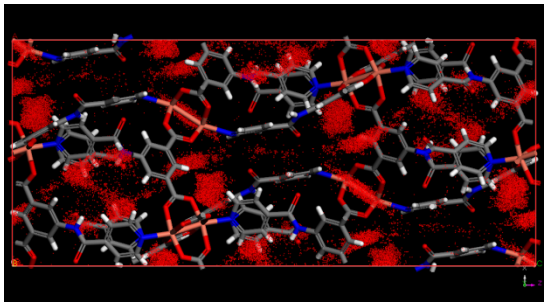	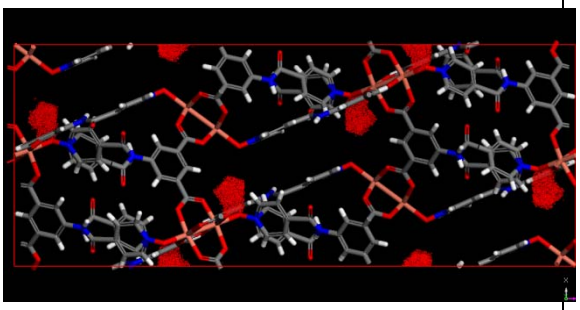
CO_2 distribution, viewed from *b* axis	CO_2 distribution, viewed from *b* axis
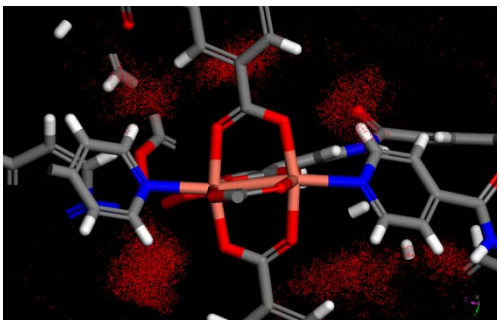	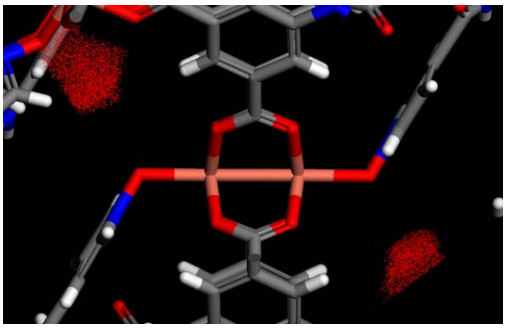
CO_2 distribution, viewed around coordination environmet	CO_2 distribution, viewed around coordination environmet

Figure S25. Distribution of CO_2 adsorbed in **LIFM-10** and **LIFM-11**

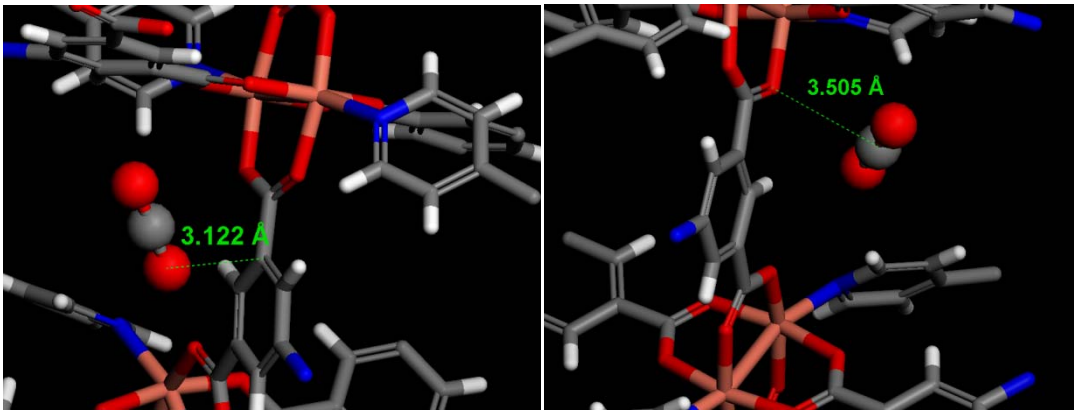

Figure S26. Preferred CO_2 adsorption site studies by annealing simulation method of **LIFM-10(Cu)**.Two main possible positionsaround the carboxylate groups and benzene ringsare obtained.

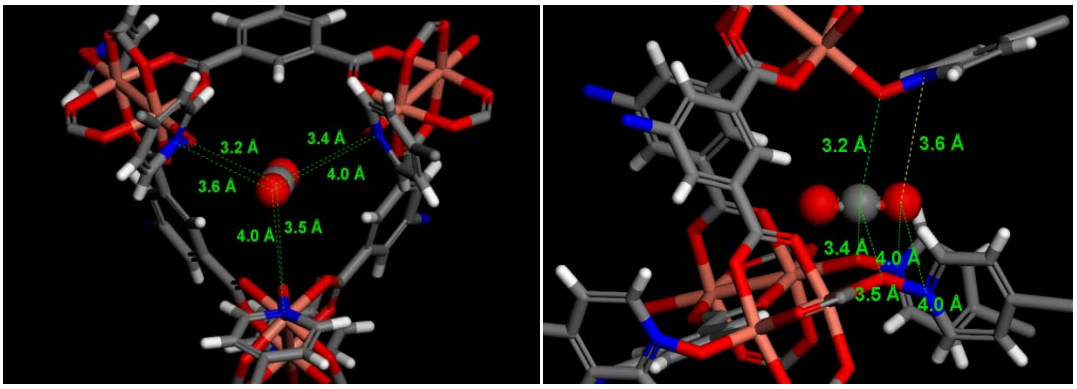

Figure S27. Preferred CO_2 adsorption site studies by annealing simulation method of **LIFM-11(Cu)**, showing different directions of mainly preferred position of CO_2.

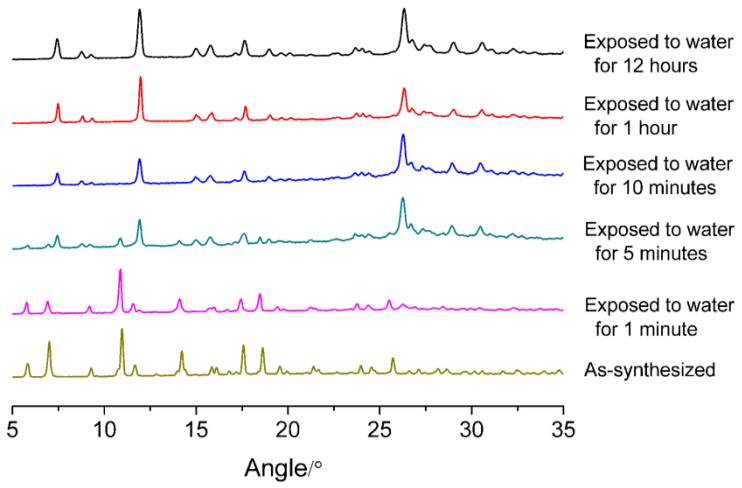

Figure S28. PXRD patterns for **LIFM-10(Cu)** immersed in water.

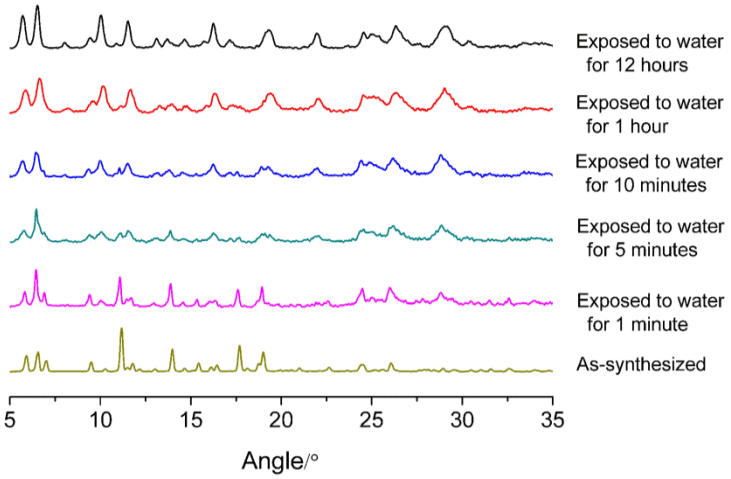

Figure S29. PXRD patterns for **LIFM-11(Cu)** immersed in water.

7. Reference

1 J. J. Ferreiro, J. G. de la Campa, A. E. Lozano, J. de Abajo, *Journal of Polymer Science Part A: Polymer Chemistry,* 2005, **43** (21), 5300-5311.

2 G. M. Sheldrick, *SHELX 97, Program for Crystal Structure Solution and Refinement*, *Göttingen University*, 1997.

3 (a) V. Blatov, A. *IUCr Comp. Comm. Newslett., 2*006, **7**, 4-38. (b) V. A. Blatova, D. M. Proserpio, *ActaCrystallogr.,* 2009, **A65**, 202–212.

4 L. Czepirski, J. Jagiello, *Chem. Eng. Sci., 1*989, **44**, 797-801.

5 A. L. Myers, J. M. Prausnitz, *AIChE Journal,* 1965, **11**, 121-127.

6 J. Jagiello, T. J. Bandosz, K. Putyera, J. A. Schwarz, *J. Chem. Eng. Data,* 1995, **40**, 1288-1292.

7 T. M. McDonald, D. M. D'Alessandro, R. Krishna, J. R. Long, *Chem. Sci.*, **2011**, **2**, 2022-2028.

8 A. Demessence, D. M. D'Alessandro, M. L. Foo, J. R. Long, *J. Am. Chem. Soc.*, **2009**, **131**, 8784-8786.

9 J. M. Gu, T.H. Kwon, J. H. Park, S. Huh, *Dalton Trans.*, **2010**, **39**, 5608-5610.

10 P. L. Llewellyn, S. Bourrelly, C. Serre, A. Vimont, M. Daturi, L. Hamon, G. D. Weireld, J.-S. Chang, D.-Y. Hong, Y. K. Hwang, S. H. Jhung, G. Ferey, *Langmuir,* 2008, **24**, 7245-7250.

11 J. An, N. L. Rosi, *J. Am. Chem. Soc.*, **2010**, **132**, 5578-5579.

12 B. Arstad, H. Fjellv_ag, K. O. Kongshaug, O. Swang, R. Blom, *Adsorption,* 2008, **14**, 755-762.

13 X. Si, C. Jiao, F. Li, J. Zhang, S. Wang, S. Liu, Z. Li, L. Sun, F. Xu, Z. Gabelica, C. S Chick, *Energy Environ. Sci.,* **2011**, **4**, 4522-4527.

14 S. R. Caskey, A. G. Wong-Foy, A. J.Matzger, *J. Am. Chem. Soc., 2*008, **130**, 10870-10871.

15 J. An, S. J. Geib, N. Rosi, *J. Am. Chem. Soc., 2*009, **131**, 8376-8377.

16 P. D. C. Dietzel, R. E. Johnsen, H. Fjellvag, S. Bordiga, E. Groppo, S. Chavan, R.Blom, *Chem. Commun.*, 2008, 5125-5127.

17 L. E. Chirlian, M. M. Francl, *J. Chem. Phys.*, 1985, **82**, 3235-3264.

18 (a) A. D. Becke, *J. Chem. Phys.,* 1993, **98**, 5648-5652. (b) C. Lee, W. Yang, R. G. Parr, *Phys. Rev. B.,* 1981, **23**, 5048-5079. (c) B. Miehlich, A. Savin, H. Stoll, H. Preuss, *Chem. Phys. Lett.,* 1989, **157**, 200-206.

19 W. R. Wadt, P. J. Hay, *J. CHem. Phys.,* 1985, **82**, 299-310.

20 M. J. Frisch, G. W. Trucks, H. B. Schlegel, G. E. Scuseria, M. A. Robb, J. R. Cheeseman, G. Scalmani, V. Barone, B. Mennucci, G. A. Petersson, H. Nakatsuji, M. Caricato, X. Li, H. P. Hratchian, A. F. Izmaylov, J. Bloino, G. Zheng, J. L. Sonnenberg, M. Hada, M. Ehara, K. Toyota, R. Fukuda, J. Hasegawa, M. Ishida, T. Nakajima, Y. Honda, O. Kitao, H. Nakai, T. Vreven, J. A. Montgomery, Jr. J. E. Peralta, F. Ogliaro, M. Bearpark, J. J. Heyd, E. Brothers, K. N. Kudin, V. N. Staroverov, R. Kobayashi, J. Normand, K. Raghavachari, A. Rendell, J. C. Burant, S. S. Iyengar, J. Tomasi, M. Cossi, N. Rega, J. M. Millam, M. Klene, J. E. Knox, J. B. Cross, V. Bakken, C. Adamo, J. Jaramillo, R. Gomperts, R. E. Stratmann, O. Yazyev, A. J. Austin, R. Cammi, C. Pomelli, J. W. Ochterski, R. L. Martin, K. Morokuma, V. G. Zakrzewski, G. A. Voth, P. Salvador, J. J. Dannenberg, S. Dapprich, A. D. Daniels, Ö. Farkas, J. B. Foresman, J. V. Ortiz, J. Cioslowski, and D. J. Fox, *Gaussian, Inc., Wallingford CT*, 2009.

21 S. Kirkpatrick, C. D. Gelatt, M. P. Vecchi, *Science,* 1983, **220**, 671-680.